

The impact of small woody features on the land surface temperature in an agricultural landscape

Fatemeh Ghafarian^{a,*}, Gohar Ghazaryan^a, Ralf Wieland^a, Claas Nendel^{a,b}

^a Leibniz Centre for Agricultural Landscape Research (ZALF), Eberswalder Straße 84, Müncheberg 15374, Germany

^b Institute of Biochemistry and Biology, University of Potsdam, Am Mühlenberg 3, Potsdam 14476, Germany

ARTICLE INFO

Keywords:

Woody features
Cooling effect
Climate
Eccentricity
Machine learning

ABSTRACT

The effects of land cover configuration on land surface temperature (LST) have been extensively documented. However, few studies have examined the effects of woody features and their configuration on LST in agricultural landscapes. A study was conducted in Brandenburg, Germany to examine the potential impacts of small woody features (SWF) on the LST of adjacent agricultural areas. High-resolution maps of woody features at the regional scale, together with the remotely sensed proxies of vegetation conditions (such as topography and crop types), were used to quantify the impact of SWFs on the gradient of LST at different distances during the dry season (June to September) of each year between 2017 and 2020. The structural characteristics of SWFs, orientation, eccentricity and size, were used as input in a multilinear regression model and in machine learning methods to predict LST at different distances. The results of the regression methods applied in this study illustrate that the surface temperature and then the eccentricity of SWFs play the key roles in predicting the gradient of LST at different distances to adjacent fields. This study determines the role of other attributes of SWFs in the prediction of LST, which will influence future landscape planning decisions and strategies.

1. Introduction

Agricultural production faces numerous challenges, including climate change and global population growth. Its bioclimatic dependency makes agriculture the most vulnerable economic sector to climate change (Hatfield et al., 2020). Negative impacts of global warming on the agricultural sector affect the provision of food for a growing human population (Dumortier et al., 2021; Godde et al., 2021; Rezaei et al., 2023). A future warmer climate raises the prospect of more intense and frequent heat waves (Meehl and Tebaldi, 2004). Contemporary cropping systems encounter significant difficulties when it comes to adapting to increasing average temperatures and, in particular, heat waves (Lüttger and Feike, 2018; Beillouin et al., 2020; Webber et al., 2020). For this reason, adaptation methods that reduce the impact of heat waves on crops are in demand.

Trees, shrubs and other perennial woody plants that grow taller than common crops have come into focus as features of the agricultural landscape that provide shade to their immediate vicinity and transpire water from a larger soil moisture reservoir, potentially offering a “cooling service” (Monteith et al., 1991; Kanzler et al., 2019; Swieter et al., 2022). Small woody features (SWF) are patchy or linear structures

of woody vegetation, such as solitaires, groves, woodlots, thickets, hedgerows, bocages or gallery forests, but considerably smaller in size than forests, although a clear size definition is lacking (Plieninger, 2011). SWFs are traditional elements in agricultural landscapes across Europe that have been historically managed for decades or centuries to provide ecosystem services such as provisioning (e.g., wood for fuel, timber), regulating (carbon sequestration, purification of air and water), and others (e.g., cultural and aesthetic) (Franz et al., 2010). Based on their spatial arrangement in the terrain, they may drastically influence local wind speeds and turbulent mixing of air masses from a microclimate perspective (Brandle et al., 2004; Heisler and Dewalle, 1988; McNaughton, 1988).

The woody features' microclimate encompasses the sub-canopy local climate, which is buffered and subsequently decoupled from the surrounding „mesoclimate“ (at landscape level) or “macroclimate” (at the regional and higher scales) due to physical protection against strong air mixing or incoming radiation (Bramer et al., 2018). Evidence suggests that tree canopies may effectively buffer understorey environments against climate extremes and support microclimates that may moderate the response of sub-canopy species to macroclimatic warming (Davis et al., 2019; De Frenne et al., 2019).

* Corresponding author.

E-mail address: fatemeh.ghafarian@zalf.de (F. Ghafarian).

The spatial arrangement of woody elements in the agricultural landscape, taking into account the field geometry, wind direction, and terrain slopes, has the potential to alter the mesoclimate of the respective area, as a result of a range of microclimatic effects (Donat et al., 2023). According to the comparable studies in this field, woody features act as a buffer for a variety of microclimate variables. Changes in the microclimate conditions are noticeable only within proximity to wooded features, within a distance approximately ten times greater than the height of the windbreak (Brenner et al., 1995; Cleugh, 1998). Yet, to our knowledge, research on the impact of integration of woody features into the agricultural landscape and how their specific microclimate affects the mesoclimate is still lacking.

To maintain a well-balanced mesoclimate within cropland, farmers have traditionally embraced the practice of cultivating woody features (Cleugh, 1998). In temperate zones, woody features are used to maintain biodiversity and provide ecosystem services, whereas in tropical and subtropical zones, agriculture and horticulture are primarily focused on using hedges to manage water and soil (Vanneste et al., 2020; Montgomery et al., 2020). Woody features are a common measure in the Mediterranean region to prevent soil erosion (Donjatee et al., 2010; Gomez-del-Campo, 2010), and provide habitat for other plant species (Bassa et al., 2012).

The characterisation of a specific mesoclimate is challenging due to its typical spatial extent of several square kilometres. Land surface temperature (LST) is one climate variable that can easily be assessed across large areas through the use of remote sensing, while the spatial patterns of air humidity, wind speed and related indicators are more difficult to obtain. In this study, we use remotely sensed LST as a proxy for the air temperature above that surface. Air temperature is then the relevant feature to assess the risk for crop underperformance (Asseng et al., 2015), animal welfare (Gauly and Ammer, 2020) and human thermal comfort (de Abreu-Harbach et al., 2015). Under low-wind speed and high-radiation conditions, the LST is a significant factor that influences near-surface air temperature (Karnieli et al., 2010; Gao et al., 2011; Good et al., 2017; Khanal et al., 2017; Keenan and Riley, 2018). We assume that LST observed over a dominantly open agricultural landscape is an appropriate indicator for the surface's radiation turnover regime and the resulting mesoclimate at the landscape scale (Mutibwa et al., 2015). The potential of SWFs to control the surrounding LST is not fully understood and has not been quantified until now. We investigate the feedback between SWFs and the gradient of LST as affected by insolation and the dominant wind speed and direction (Tamang et al., 2010; Baker et al., 2021). For this purpose, we break down the effects of SWFs on temperature gradients by their physical properties, size, type, orientation and eccentricity.

To evaluate the effects of SWFs on the LST of nearby agricultural fields, remote sensing (RS) data has been supplied sufficient details from the plant conditions (Senay et al., 2019; Weiss et al., 2020) and assess heat and water stress (Sayago et al., 2017; Virnodkar et al., 2020; Zhu and Burney, 2022). The Copernicus Land Monitoring Service provides homogeneous information on SWFs at the European level using Very High Spatial Resolution (VHSR) Earth Observation (EO) scenes (Copernicus, 2019). In this study, we used the available high-resolution maps of woody features at the regional scale, together with the remotely sensed proxies of vegetation conditions (such as topography and crop types), to examine the effects of SWFs on the nearby field's climate from the standpoint of LST.

Given the significance of the preceding facts, the overarching goal of this study is to illustrate whether an SWF has a significant impact on the LST of adjacent fields. We also aim to shed light on the structural and dynamic attributes of SWFs, which would affect the temperature gradient of the landscape. To this end, we compare the results of multilinear regression and machine learning methods to predict LST at different distances from an SWF.

2. Methods

2.1. Case study

The area under investigation is the rural district (*Landkreis*) of Märkisch-Oderland (MOL), located in the Federal State of Brandenburg, Germany (52°N, 13°E; Fig. 1a). The overall topography of the region is dominated by softly rolling hills, generally with altitudes between 100 and 150 m above mean sea level (a.s.l.). Agricultural land accounts for approximately 45 % of the area of the Federal State of Brandenburg, totalling 29,640 km² (Amt für Statistik Berlin-Brandenburg, 2016). According to Köppen's classification, Brandenburg's climate is characterised by a warm humid continental climate (Dfb) with warm summers (Kottek et al., 2006). Mean annual precipitation is 521 mm (max. = 749 mm in 2010, min. = 348 mm in 2004), with a mean annual temperature of 10.0 °C for the period 1991–2020 (max. 11.8 °C, 2014; min. 8.5 °C, 2004), as observed at the Müncheberg meteorological station. These conditions, paired with sandy soils of very low water holding capacity, pose considerable challenges to agricultural production.

2.2. Input data

2.2.1. Land surface temperature

Land surface temperature (LST) was derived from satellite remote sensing data (Landsat 8). For this purpose, we used LST retrieval method based on single thermal infrared (IR) channel to investigate the thermal gradients of SWFs in adjacent fields. 30 m spatial resolution data was retained for the derived LSTs, although the landsat thermal bands are resampled from their original 100 m resolution. In this method, the algorithm also used other bands, such as NIR and R, which have 30 m resolution. The LST was obtained during the warmest period in Brandenburg between 1 June and 1 September for four years (2017, 2018, 2019 and 2020). The LST was collected throughout this time, and images from 49 time steps were analysed. All the images of the MOL region were captured between 10:50 and 11:05 am in the local time zone (CEST). The algorithm for estimating LST was developed in Google Earth Engine based on a Statistical Mono-Window (SMW) algorithm (Ermiida et al., 2020). The images with less than 20 % of cloud cover were selected. In addition, Landsat Pixel Quality Assurance information was used to mask out any pixels with lower quality such as pixels with cloud or cloud shadows. In the final step, Landsat LST data for each year were aggregated using mean in order to have continuous coverage over the study area. Subsequently, the LST data were resampled to a 5-meter resolution, aligning with the reference resolution established in this study through the 'Nearest Neighbour' method. The resulting cell's value is established based on the closest cell centre within the input grid.

2.2.2. Small woody features

The Small Woody Features (SWF) layer, used by Copernicus to determine tree and shrub coverage in German agricultural areas, comprises woody linear and small patchy elements. These elements adhere to specific geometric specifications, with patches and additional features having minimum and maximum areas of 200 and 5000 m², respectively (Copernicus, 2019).

The Copernicus Land Monitoring Service provides SWFs at the pan-European level using more than 37,000 very High Spatial Resolution (VHSR) Earth Observation (EO) scenes. The main outputs of this extraction are vector and raster products (5 m and 100 m spatial resolution) (Fracqueur et al., 2019), which provide homogeneous information on the structure of SWFs, such as linear features (hedgerows, bocages, lines of trees, etc.) and small patches of woody vegetation (solitaires, groves, thickets, woodlots, etc.), for the reference year 2015 (± 1 year) (Copernicus, 2019). This dataset is publicly available on a large scale for agricultural areas in Brandenburg.

The map of SWFs in MOL was re-projected to EPSG 3035 with a 5 m resolution. This specific projection and resolution are considered as the

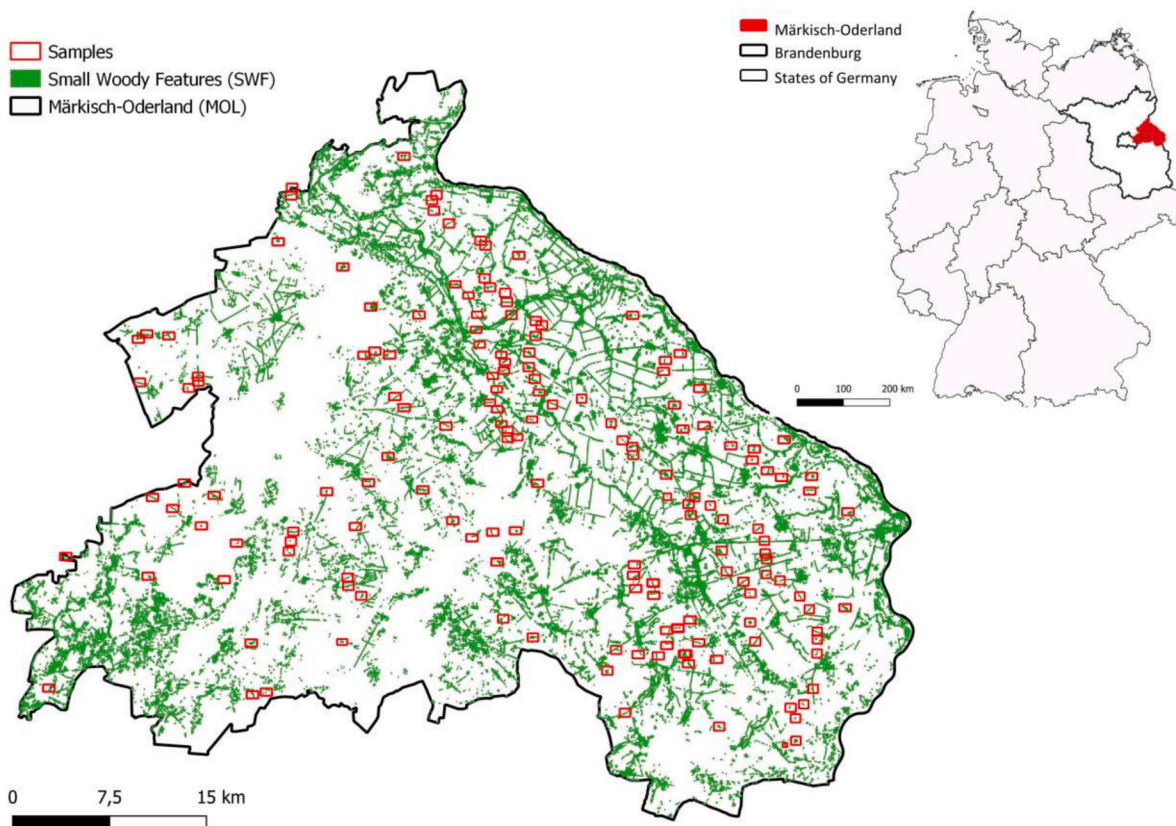


Fig. 1. The study area (*Landkreis Märkisch-Oderland*, a rural district located in the Federal State of Brandenburg, Germany) showing small woody features (green pixels) and the selected sample sites (red rectangles).

reference standards for processing other maps (LST, crop types, and distance maps) throughout our research. The final processed map of SWFs was then used to randomly select 135 samples from the agricultural area of MOL. Each sample covers an area of 50 to 52 hectares, including one to a maximum of six different SWFs, preferably located in the centre of the sample (see Fig. 1). The selected samples of the SWF map were used as the reference map to select the same area of other maps, LST, crop type map, and elevation, and to resample and re-project them in this study.

2.2.3. Crop type map

Multi-year agricultural land cover maps based on study of Blickensdörfer et al. (2022) were used in our study. Their approach involved applying a random forest classifier and dense time series data from Sentinel-2 and Landsat 8 in combination with monthly Sentinel-1 composites and environmental data. The mapped area, containing major crop sequences of cereals and leaf crops, has adequate accuracy (78 % to 80 %) and is aligned well with agricultural statistics at the regional and national levels. Blickensdörfer et al. (2022) classified and tested 24 agricultural land cover classes in Germany for the period from 2017 to 2020, in which the meteorological conditions differed significantly. Based on the output of that work, binary masks of winter and spring crops were created.

Prior to the analysis, all maps used in this study were re-projected and resampled to the reference map. For each sample, we determined the SWF types and crop types in adjacent fields. Based on the cropping patterns in the study area, we used broad categories of cropland management, i.e. spring crops (maize, oilseed rape, oat and soybean) and winter crops (rye, wheat, oilseed rape and winter barley), as well as grasslands.

2.2.4. Distance map

SWFs are highly scattered throughout various landscapes, causing challenges for the selection process. To address this, we selected a cluster of SWFs, preferably situated at the centre of each sample (as shown in Fig. 2). Notably, in each sample, the group of SWFs is positioned in such a way that, at least in one direction, it remains disconnected from the next group of SWFs. For instance, in Fig. 2, there are no SWFs to the West, East, and South of the group, while a single SWF is situated to the North of the group.

The data is retrieved from the centroid point of each SWF and moved pixel by pixel in four primary directions. We excluded pixel values in directions where they intersected with another group of SWFs within the sample. This decision was made to ensure that we could estimate the impact of only one SWF on LST in each direction. We used OpenCV, an open-source Python library (Villan, 2019), to process SWF images comprising only woody features with a resolution of 5 m and to generate a distance map with the same resolution for each sample. In this approach, all pixels receive a value based on their distance to the border of the nearest SWF, dependent on the position of the SWFs in the sample. Pixels located inside the SWFs are assigned a value of zero (see Fig. 2) and as one moves away from the SWFs, the pixel values increase, representing a gradual distance from the SWFs.

2.3. The warming or cooling impacts of small woody features on land surface temperature

Considering only pixels that were not influenced by any other SWF, we used the distance map, the multi-year LST map, the crop rotation map (2017 to 2020) and digital elevation model (see Fig. 3) for further analysis. Fig. 3 shows an example of the values available from the LST map and the crop map for the year 2017 in the westward direction of a single SWF in one of the samples.

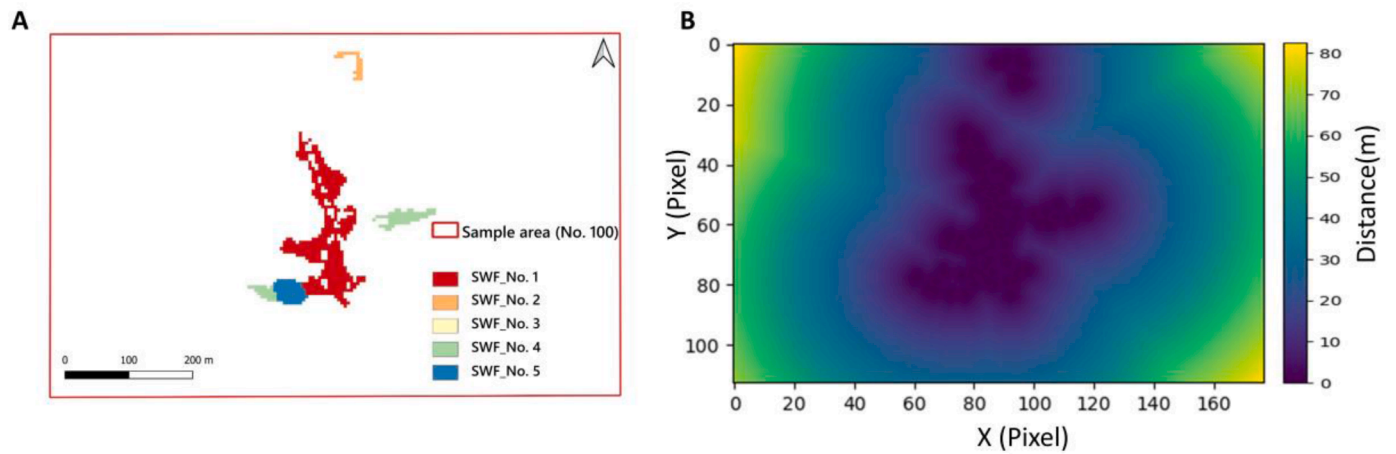


Fig. 2. A random sample of SWFs with a resolution of 5 m, consisting of five distinct SWFs, each labelled with a different colour (A). The distance map in [m] generated based on the locations of the SWFs in the sample, showing the minimum distance between the SWFs (B).

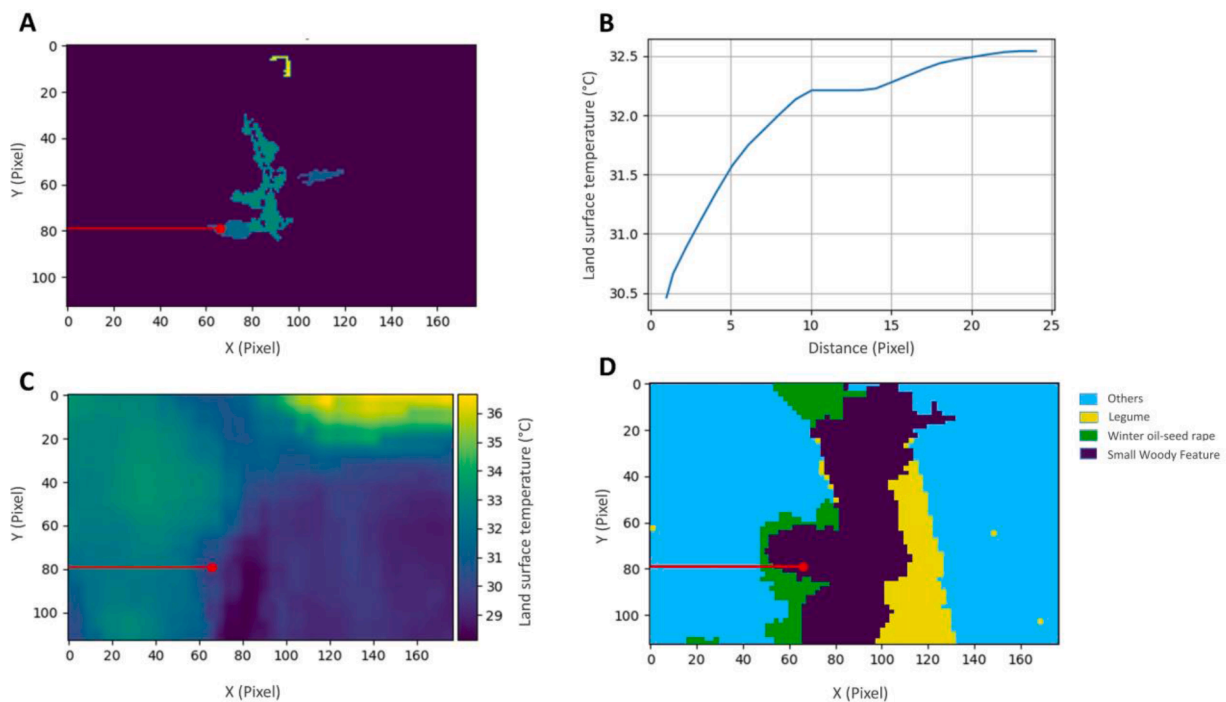


Fig. 3. Overview of remote sensing and auxiliary data for a sample small woody feature (SWF; ID: 65). From the centroid point of the SWF (red dot) in the SWF map (A), we moved pixel by pixel (red line) towards the west, after having assured that there was no other SWF in this direction. The correlation between distance and LST is plotted (B). The values for surface temperature and crop type for each pixel were obtained from the LST map (C) and the crop map (D), respectively. This procedure is then repeated in northerly, easterly and southerly directions.

We then set up a dataset for each sampled SWF containing all its attributes as defined by Copernicus (2019), e.g. size and type, as well as additional attributes obtained from image processing. We defined additional attributes to the SWF, including orientation and eccentricity. Regarding the aspect of an SWF functioning as a windbreaker, it was expected that more details about the shape and orientation of the SWF would better explain its cooling effect. Orientation is the angular position of a reference line from east (0°) to west (180°) of an asymmetric SWF. In this study, we considered an imaginary east-west line as a reference, stretching throughout the woody feature from a reference placement to its current placement.

The eccentricity (e) of an SWF describes its deviation from a perfect

circular shape. It is defined as $e = \sqrt{1 - \frac{b^2}{a^2}}$, where a and b are semi-minor axes and $a > b$. An ellipse with equal axes has zero eccentricity, and is a circle. The more elliptic the SWF is, the greater the value of its eccentricity. At the opposite extreme, a value of 1 describes a linear SWF.

The LST maps for all years had a resolution of 5 m. From a series of moving points starting from each centroid point towards different directions, points with distance values of less than 25 m were considered as the average LST of an SWF (LST_{SWF}).

$$LST_{SWF} \sim LST [0 \text{ pixel} = < \text{distance value} < 2 \text{ pixels}]$$

There was no significant difference between the LST and their

gradients of the four cardinal directions. We therefore did not consider the individual directional data any further. For the distance from the centroid point of the SWF in any direction, we defined four different distance zones: Zone 1 – less than 25 m (1 to 5 pixels); Zone 2 – between 25 m and 50 m (5 to 10 pixels); Zone 3 – between 50 m and 75 m (10 to 15 pixels); and Zone 4 – between 75 m and 100 m (15 to 20 pixels). We further defined Zone 4 as the reference LST (LST_{Ref}), assuming that it represents an LST that is not affected by an SWF (see Table 1). For each sample, the values of LST at each point were deducted from LST_{Ref} in each direction, making sure that there was no overlap with the influencing zone of another neighbouring SWF. The difference between two temperatures ($LST_{point} - LST_{Ref}$) is defined as the cooling effect of an SWF.

The length of the distance moving from centroid points towards different directions varied for each SWF due to their size and shape, their location in the sample, and the sample size. We therefore chose the minimum length of 20 pixels (100 m) for all centroid points, and preferred samples in which the SWF was positioned centrally. If the sum of the differences in LST between each point's LST and SWF ($LST_{point} - LST_{Ref}$) is negative within 20 pixels, the LST experiences a cooling effect due to the SWF, while a positive sum represents a higher LST in the vicinity of an SWF, indicating a warming effect. From the database, outliers were reduced due to a lack of information on LST in some pixels. Table 1 summarises the entire information about the area around the SWFs at defined distances.

To study temperature variation at different distances, we formulated a hypothesis based on LST data within 100 m for each pixel in the four cardinal directions, with the SWF at the centre. This hypothesis allowed us to provide a testable prediction, a critical aspect of our method. In our study, the null hypothesis (H_0) assumes similarity in LST distributions for various distances from the SWF, while the alternative hypothesis (H_a) assumes no similarity in LST distribution across distances. Null hypothesis significance testing (NHST) was used to test the rejection of H_0 with a 95 % confidence level (Fisher, 1925). To this end, the datasets were uniformly reduced to a size of 1000 samples. First, a Shapiro–Wilk test checked for normal data distribution. Then, using an ANOVA across all years, Welch's t -test examined the influence of direction and zone, facilitated by Python modules "scipy.stats" and "statsmodels" (Skipper and Perktold, 2010). Levene's test assessed the equality of variances at different distances.

2.4. Machine learning methods

We used hypothesis testing to investigate any similarity in the behaviour of SWFs at different distances. We ran a multilinear regression model (MLR) with three other regression models (Extra Trees Regression (ETR), Random Forest Regression (RFR) and Gradient Boosting Regression (GBR)) to predict the LST of the adjacent field at a short distance. All computations for this study were run on Python (version 3.6.8).

Multiple linear regression (MLR) is a conventional and widely used approach for estimating temperature (Zhang et al., 2019). Recent studies have demonstrated that machine learning models are also well

suitable for temperature prediction (Pouyan et al., 2022). In this study, both types of models were used to investigate how well the physical attributes of SWFs can be used to predict LST in adjacent field. Three data-driven algorithms for predicting were introduced in this section. These algorithms include extra trees (ET), Random Forest Regression (RFR), and Gradient Boosting Regression (GBR). In our study, we used the coefficient of determination metrics (R^2) and the mean absolute error (MAE) as common metrics to evaluate training and validation of the model.

2.4.1. Multilinear regression (MLR)

In the MLR model, the relationships between a dependent variable (LST in different distances from SWF in this study) and two or more independent variables (e.g., the proposed 4 physical features of SWF and crop types) are established using the linear function. We checked the correlation coefficient between each feature and LST, and ranked the features from high to low according to the coefficients.

2.4.2. Random forest regression (RFR)

As a tree-based ensemble method, it was developed to address the shortcomings of traditional Classification and Regression Tree method. RFR consists of a large number of weak decision tree learners, which are grown in parallel to reduce the bias and variance of the model at the same time (Breiman, 2013). For training a random forest, N bootstrapped sample sets are drawn from the original dataset. Each bootstrapped sample is then used to grow an unpruned regression (or classification) tree. The most important hyperparameters to tune for the RF are $n_{estimators}$, $max_samples$, $n_{features}$, and max_depth (see Table S1).

2.4.3. Extra trees regression (ETR)

The Extra Trees algorithm is a machine learning technique that extends the random forest algorithm. It is designed to reduce overfitting in datasets (Geurts et al., 2006). Similar to random forest, Extra Trees trains each base estimator with a random subset of features (John et al., 2016). However, during the process of splitting nodes, Extra Trees selects the best feature and its corresponding value randomly. In contrast, random forest trains the model using bootstrap replicas. This randomness in feature and value selection makes Extra Trees less prone to overfitting compared to random forest (John et al., 2016). Each regression tree in Extra Trees is trained using the entire training dataset (for the results of tuning in Table S2).

2.4.4. Gradient boosting regression (GBR)

Like any other regression problem, in GBM too we try to find a regression function, fb that minimizes the loss function (for example, squared error loss) but with a weak learner (for example, regression trees) (Kuhn and Johnson, 2013). Regression trees are excellent choice for base learners in GBM algorithm because they are easy to prune (require only one parameter, tree depth), can be added together to form an ensemble and are computationally fast (Ridgeway, 2007). Two tuning parameters (tree depth or interaction depth and number of iterations) are typically adjusted for model training.

Table 1

Summary of data for the area around small woody features (share of data, mean land surface temperature (LST), its standard deviation (SD), minimum LST, and elevation in seven distances classes (zones) for four years 2017–2020).

Zone	Distance [m]	Share of data [%]	Mean LST [°C]	SD [K]	Min LST [°C]	Elevation [m]
Zone 1	0–25	15.0	36.6	4.5	25.6	33.7
Zone 2	25–50	14.3	37.4	4.6	25.8	32.7
Zone 3	50–75	14.1	37.8	4.8	25.8	33.0
Zone 4	75–100	15.2	38.0	4.9	25.4	33.8
Zone 5	100–125	14	38.1	5	25.2	33.3
Zone 6	125–150	13.7	38.1	5.2	25.6	33.7
Zone 7	150–175	13.7	38.1	5.2	25.4	33.4

2.5. The impact of small woody features on land surface temperature at different distances

The values of differences in LST at each distance from the SWF were considered for each pixel. In each direction from the SWF, we estimated the accumulation of differences in LST values at different distances from the SWF using rolling linear regression models, with a fixed window of time over the entire dataset. Given the length limitation of the observations for each direction (20 pixels), we considered a minimum length of 6 pixels to obtain larger parameter estimates. These accumulation values were later considered at 25 m, 50 m, 75 m and 100 m, and their values represent the impacts of the SWF at those distances. If the gradient of LST in Zone 4 as a reference point towards the SWF is negative, it implies that the cooling effect of the SWF gets stronger towards the SWF. Conversely, a positive value means that LST gets warmer when approaching the SWF.

3. Results

3.1. Overall changes in land surface temperature for different distances to small woody features

The values of SWF generated as described in Section 2.3 were organised in a dataset. Statistical tests for normality (Shapiro and Wilk, 1965) were applied to check if the values from each sample have a normal distribution in different directions and at different distances. Furthermore, violin plots (Fig. 4) show the distribution of LSTs in the four distance zones for each individual year. The year 2018, an extraordinarily warm summer in Germany, produced the highest LST (40.5 °C) and the largest amplitudes (24.3 K). The absolute LST increased from the centre of the SWFs outwards, at different temperature levels each year, but always with a similar gradient. On average, the LST in Zone 2 was +0.8 K higher than the LST in Zone 1, followed by Zone 3 (+1.5 K) and Zone 4 (+1.8 K).

Table 2, showing the average LST for all zones, illustrates an increase in the values of surface temperature by changing zones and moving towards Zone 4, where LST was considered the reference point. This table clearly demonstrates that the differences in LST between Zone 4 and the other zones were higher in Zones 1 and 2 than in Zone 3.

Bold figures in Table 2 shows where the null hypothesis (H₀) was rejected based on the result of the t-test, which suggests that there is a significant difference between the LST in Zone 1 and that in other zones. For Zones 3 and 4, H₀ was rejected in all years; for Zone 2, it was significant only for the year 2017.

The temperature difference between each point and the reference points outside the SWF in Zone 4 indicates whether or not we are experiencing a cooling effect at that point. In the case of a cooling effect, this difference is negative. Across our region, the average yearly

Table 2

The average absolute land surface temperature (LST) for each zone in four consecutive years (2017–2020) in [°C].

Zone	2017		2018		2019		2020	
	Mean	SD	Mean	SD	Mean	SD	Mean	SD
Zone 1	32.7	2.1	40.9	3.4	37.3	2.8	39.3	2.9
Zone 2	33.6	2.2	41.8	3.5	38.2	2.8	40.1	3.0
Zone 3	34.2	2.3	42.5	3.6	38.8	2.9	40.8	2.9
Zone 4	34.5	2.3	42.8	3.7	39.1	3.0	41.2	2.9

temperature differences in the four defined distance zones (0–25 m, 25–50 m, 50–75 m and 75–100 m) were –1.0, –0.7, –0.2 and 0.0 °C, respectively. 77.6 % of differences in LST experienced a higher LST when moving away from the SWF, while 22.4 % of the adjacent fields had a lower LST than the nearest SWF.

3.2. Variations of the impact of crop types on land surface temperature

Based on the crop categories defined in Section 2.2.3, the order of dominant cultivated crops in the fields where a warming effect was observed was: winter crops (9.6 %), followed by grassland (5.4 %) and spring crops, mainly maize (6.2 %). In cases where a cooling effect was observed, winter crops (55.2 %) and then spring crops (8.7 %) had the highest percentages of land cover, and had a higher LST than the SWF of 2.2 K and 1.9 K, respectively, on average. Grasslands with a land cover percentage of (12.2 %) had a 1.9 K higher LST than the SWF on average. In this region, maize represents about 79 % of the category of spring crops, and its LST was 0.3 K higher than that of the other spring crops in this category (for more details, see Figure S2 in the supplementary material).

In the case of a warming effect, grasslands (3 K) and then spring crops (1.3 K) experienced a higher LST than their reference points in our samples. However, fields with winter crops experienced the highest cooling effect (–2.2 K), followed by fields with both winter and spring crops (–1.9 K). During this period of the year, only very little land (0.1 %) was cultivated with all of the crop types under consideration (spring and winter crops, and grassland), but those fields experienced a –1.5 K cooling effect on average.

3.3. Prediction of land surface temperature around small woody features

The methodologies utilized in this study necessitate a certain level of hyperparameter customization within the model framework. Hyperparameters were chosen independently for each utilization of the machine learning models. For the majority of hyperparameters, we stuck with the default values provided by the package. It's worth noting that the performance of GBR, RFR, and ETR did not display significant sensitivity to hyperparameter tuning. As a result, we primarily adhered

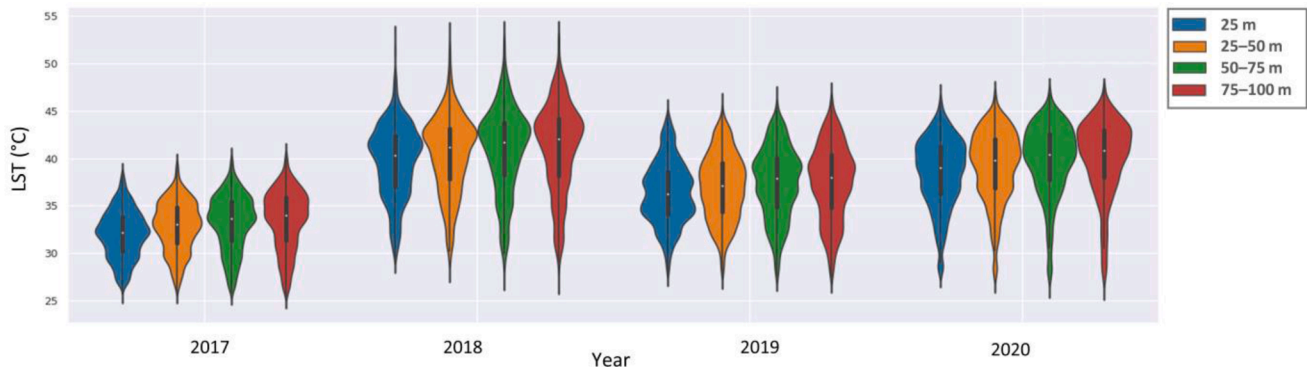


Fig. 4. The distribution of land surface temperature (LST) across four different distances (0–25 m, 25–50 m, 50–75 m and 75–100 m) during the warm period (June, July and August) of the individual years 2017, 2018, 2019 and 2020.

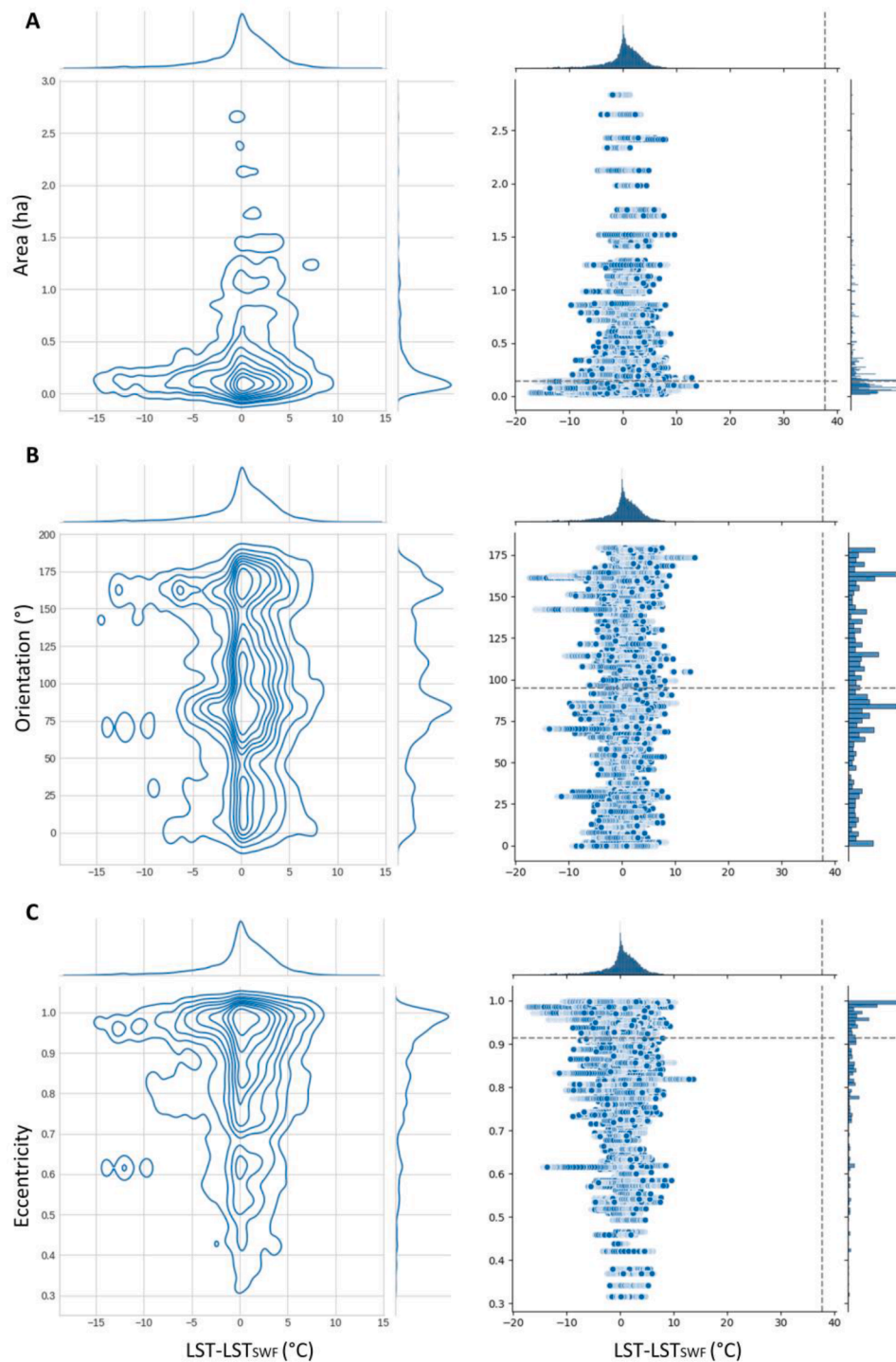


Fig. 5. The densities and distributions $LST-LST_{SWF}$ ($^{\circ}C$) and the attributes of SWFs (A: area, B: orientation, and C: eccentricity) for all samples.

to the default values (see the Tables S1–3 for more details in supplementary materials).

Fig. 5 summarizes all the characteristics based on the eccentricity and orientation that were considered in this study, together with the SWF’s size. The average eccentricity of SWFs was 0.8. However, 73 % of SWFs had an eccentricity greater than 0.8, and in 27 %, it was less than 0.5. Regarding the size of SWFs, 85 % of them were smaller than 0.5 hectares. All SWFs exhibited nearly equal distribution of orientation across three distinct groups ($0^{\circ}-40^{\circ}$, $50^{\circ}-130^{\circ}$, and $150^{\circ}-175^{\circ}$), with an average orientation of 96.6° (Fig. 5).

At this point, the physical attributes of SWFs, area, orientation and

eccentricity, along with the LST of the SWF and crop types in the fields next to the SWF were used as input for the regression models to predict the LST of the adjacent field in different zones. Regarding the four zones defined in the study, we followed two approaches to predict the LST of each zone. In the first approach, we predicted the LST of all zones based on the relevant LST of the SWF and the information available on the fields adjacent to the SWF. In the second approach, instead of using the LST of the SWF, we used as input data the LST of the next closest zone to the SWF. The coefficient of determination metrics (R^2) and the mean absolute error (MAE) were used to evaluate the performance of the models in a regression analysis. The results of all metrics for both

Table 3

Results of the regression models using LST_{SWF} as input for regression models to predict LST in different zones (Approach 1).

		2017		2018		2019		2020	
		R ²	MAE						
LST _{Zone2}	ETR	0.92	0.51	0.95	0.57	0.93	0.58	0.95	0.54
	GBR	0.92	0.57	0.95	0.60	0.92	0.62	0.94	0.57
	RFR	0.92	0.56	0.95	0.58	0.92	0.63	0.94	0.57
	Linear	0.92	0.54	0.95	0.61	0.93	0.61	0.94	0.60
LST _{Zone3}	ETR	0.87	0.68	0.92	0.81	0.83	0.97	0.87	0.83
	GBR	0.87	0.74	0.91	0.87	0.78	1.08	0.87	0.84
	RFR	0.87	0.73	0.91	0.87	0.81	1.04	0.86	0.86
	Linear	0.86	0.78	0.89	0.94	0.82	1.03	0.87	0.92
LST _{Zone4}	ETR	0.84	0.77	0.93	0.84	0.75	1.20	0.86	1.01
	GBR	0.84	0.85	0.92	1.00	0.76	1.23	0.85	1.10
	RFR	0.83	0.83	0.92	0.92	0.75	1.23	0.86	1.03
	Linear	0.79	0.96	0.91	0.93	0.80	1.21	0.82	1.24

Table 4

Results of the regression models using the land surface temperature of each zone (LST_{Zone}) as input for regression models to predict the land surface temperature of the next furthest zone (Approach 2).

		2017		2018		2019		2020	
		R ²	MAE						
LST _{Zone2}	ETR	0.92	0.51	0.95	0.57	0.93	0.58	0.95	0.54
	GBR	0.92	0.57	0.95	0.60	0.92	0.62	0.94	0.57
	RFR	0.92	0.56	0.95	0.58	0.92	0.63	0.94	0.57
	Linear	0.92	0.54	0.95	0.61	0.93	0.61	0.94	0.60
LST _{Zone3}	ETR	0.94	0.39	0.97	0.41	0.90	0.63	0.96	0.42
	GBR	0.95	0.39	0.98	0.41	0.91	0.60	0.96	0.44
	RFR	0.96	0.38	0.97	0.47	0.91	0.61	0.96	0.47
	Linear	0.96	0.38	0.97	0.45	0.92	0.54	0.95	0.46
LST _{Zone4}	ETR	0.98	0.25	0.99	0.36	0.98	0.33	0.98	0.37
	GBR	0.98	0.30	0.99	0.37	0.98	0.36	0.98	0.44
	RFR	0.97	0.32	0.99	0.37	0.98	0.33	0.98	0.40
	Linear	0.98	0.27	0.99	0.30	0.98	0.32	0.98	0.40

approaches are presented in Tables 3 and 4.

In the first approach where we considered LST_{SWF} to predict the LST of other zones, we observed no significant changes in R², but there was a particular increase in MAE in another metric (on average 33 % higher from Zone 1 to Zone 2 and 14 % from Zone 2 to Zone 3, respectively). This increase was even higher after 2018 and in the following years. In the second approach, this pattern was reversed: in the model to predict the LST of Zone 4, MAE declined specifically (on average, MAE was 27 % lower in Zone 2 than in Zone 1 and 38 % lower in Zone 4 than in Zone 3).

Multiple linear regression equations to predict LST in different zones

are used in combination with the following formulae containing six different independent variables (the temperature, orientation, eccentricity, size and direction of the SWF, and the current crop types grown in the field), with one regression coefficient for each independent variable.

$$Y = \beta_0 + \beta_1 X_1 + \beta_2 X_2 + \dots + \beta_n X_n \tag{1}$$

To predict LST at different distances, we analysed the coefficients of the MLR model, which indicated the highest positive response (1 ± 0.05) of LST_{SWF} and the lowest response to the size of the SWF in both

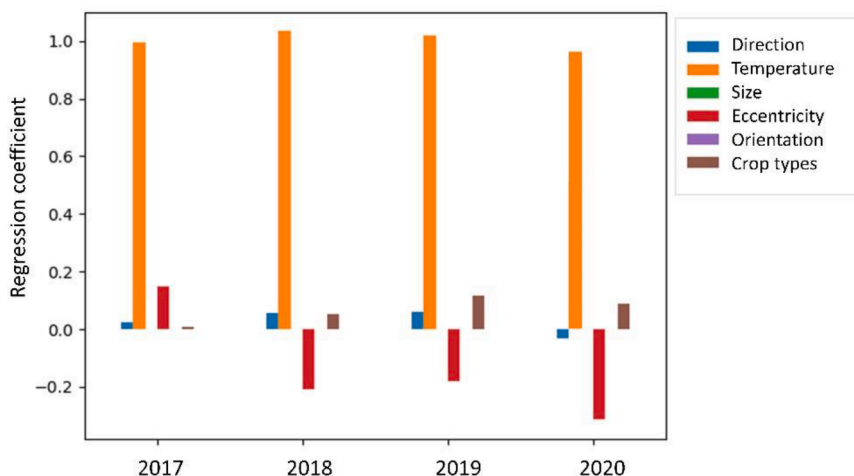


Fig. 6. The average coefficient of all independent variables (attributes of SWFs) of the multilinear regression model for both approaches.

approaches (see Fig. 6). Eccentricity is the second-most important attribute that influenced the prediction of LST (an average of -0.10). Its coefficient was positive in 2017 (an average of $+0.10$), but became negative from 2018 onwards (an average of -0.25). The coefficients of crop types averaged at 0.07 , differing in all years. In 2017, crops had the lowest impact on LST (an average of 0.01), but this value increased in the following years (0.05 , 0.1 and 0.1 , respectively). The directions of the SWF responded differently each year. In 2018 and 2019, the coefficients of the direction were high (an average of 0.06), and were lower in 2017 and 2020 (an average of 0.02 and -0.03 , respectively) (see Table S4, 5 in the supplementary materials).

This analysis was also amended for two machine learning (ML) models (GBR and RFR) by applying a SHapley Additive explanation to show the interaction effect of variables and individualised feature attributions for all years (Fig. 7). In 60 % of cases, the results of the summary plots of GBR and RFR showed that the order of influence was LST_{SWF} , size, eccentricity, orientation, crop types, and direction in both

approaches. In some cases, the direction of the SWF had a greater impact than crop types.

4. Discussion

The results indicate that the physical attributes of SWF affect the magnitude of the LST of adjacent fields. By explicitly describing the quantitative relationships of LST with the configuration of the SWF, this research expands our scientific knowledge of the effects of SWF patterns on LST in agricultural landscapes.

4.1. The impacts of crop types in the field on land surface temperature

The average LST in adjacent fields at different distances from the SWF depends on the types of crops grown, as well as their growth stages. In the region under investigation, 64.8 % of the fields contained winter crops. The photosynthetic activity of the winter crops declined in July,

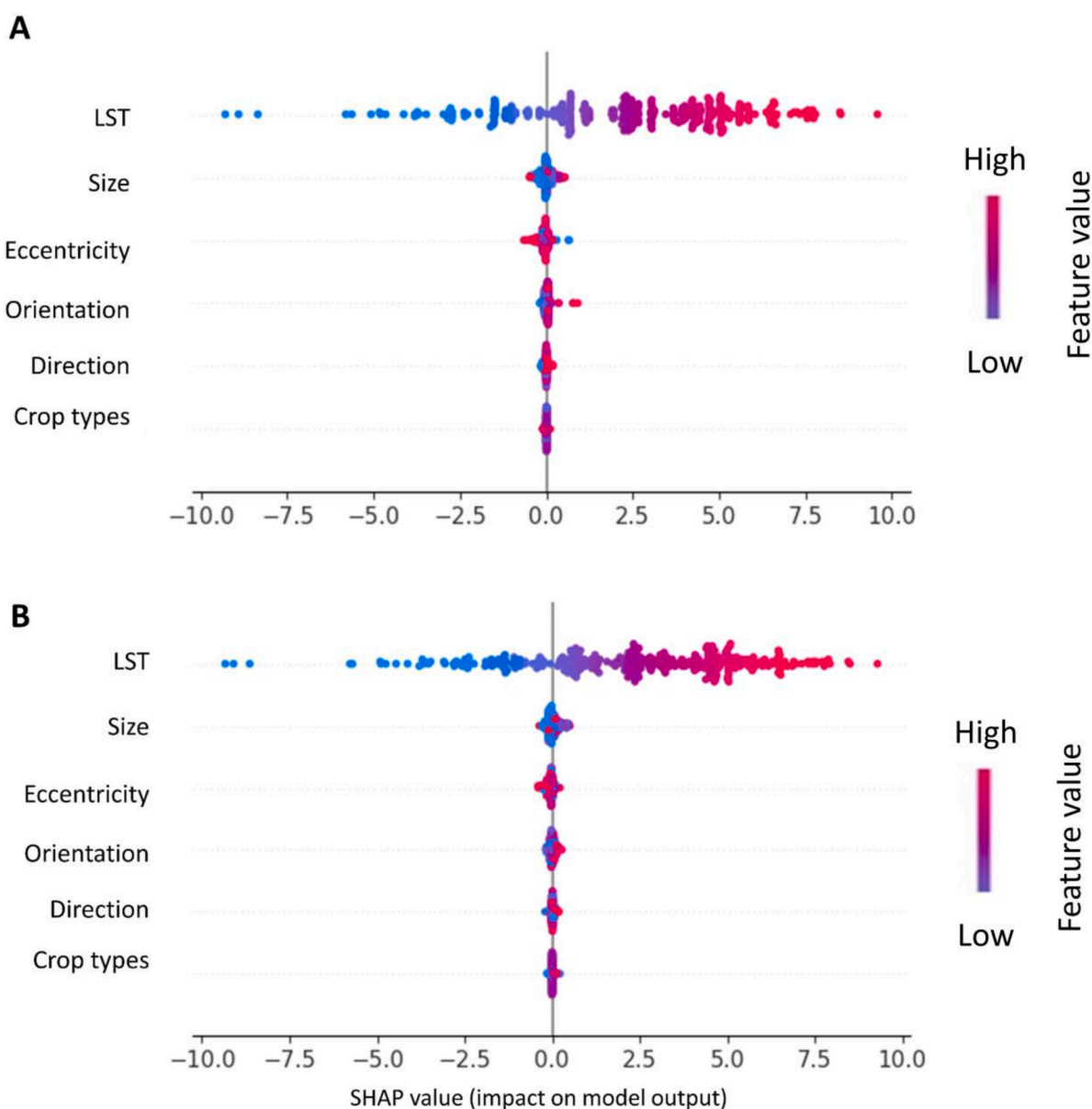


Fig. 7. SHAP summary plot with positive and negative relationships of predictors with the target variable, showing six features for the warm period (June, July and August) of years 2017 to 2020. LST_{SWF} is used as input to predict the temperature in Zone 2. (A) Summary plot of Gradient Boosting Regression (GBR) and (B) summary plot of Random Forest Regression (RFR).

as did transpiration, which cools the surface of the crop. In August, almost all of the crops had senesced. Consequently, fields containing winter crops during this period experienced a higher LST than the adjacent SWF because cooling through transpiration had ceased for crops, whereas the SWF, featuring deeper permanent roots, may still have transpired water from deeper soil layers.

Conversely, spring crops – the minor subject of this study (14.8 %) – experienced their developed and mid-stage growth mainly in June and July. 80 % of the spring crops were maize; compared to other crops in this category, these crops had a 2.1 °C higher LST than the next SWF. Maize has a longer growth cycle, which begins in May and ends after August. In June and July, therefore, maize is in its most active development stages, with maximum photosynthesis and transpiration rates. Land used as grassland, with 17.6 % land coverage of the fields, also experienced a higher LST than the SWF in most cases. In 5.4 % of the grassland, LST was lower than the SWF, which could be due to the implementation of extensive grassland management or to geographical conditions. This type of land use in Brandenburg is mainly found in low-elevation areas close to groundwater with a favourable water balance, and to a lesser extent in sandy and loamy upland soils (Kaiser et al., 2010).

Fields with both winter and spring crop types had a lower LST than the SWF compared with each of these individual crop types. This could be explained by the overlapping of their growing stages, leading to a vegetation cover on the surface throughout the warming period. Tree–soil–crop interactions in agroforestry systems are a complex mixture of positive and negative effects both above and also below ground (Kho et al., 2001). Another factor to take into account is the scale of the data we are dealing with, which is regional. This can potentially lead to disparities between field-level observations and regional-scale data (Good et al., 2017). In our analysis, we are focusing on temperature derived from satellite imagery, however, it's important to note that measurements taken beneath the canopy may reveal lower temperatures, primarily influenced by factors like solar radiation and surface conditions. Types of crops and field management could increase or decrease the potential impacts of SWFs on LST. This needs to be investigated more specifically on a regional scale, using more data on the types of cultivated crops and soil water content.

4.2. Evaluation of the different regression methods to predict land surface temperature at different distances

Our results demonstrate that the surface temperature of an individual SWF is the most important attribute for predicting LST at different distances compared to the other physical attributes of SWFs. This factor also reflects morphological features of SWFs (e.g. compactness and height of tree canopies), which could reduce the transmission of solar radiation to the understorey (Bonan, 2016). In addition, tree height is potentially coupled with the canopy effect in SWFs and the provisioning of overstorey cover (Vanneste, et al., 2020). Depending on the orientation of the tree, its height plays a relevant role in the gradient of the LST at a close distance to the SWF (Montgomery et al., 2020). The results of the statistical analysis indicated that the LST in Zones 1 and 2 experienced similar LST distributions, while from Zone 3 onwards the effect of the SWF becomes smaller. This testifies to evidence that temperature has an effective impact up to 50 metres from the SWF.

In both of the approaches applied, the area covered by an SWF made a major contribution to the prediction of LSTs using machine learning methods. This fact was also confirmed in the statistical analysis of fields to the south of the SWF, with almost double the area experiencing a lower LST on this side and the highest LST gradient. This means that the larger area was able to increase the positive impacts of the SWF on adjacent fields. However, this feature had the lowest positive impact on the MLR. This fact may lead us to consider other physical attributes of SWFs that could play a larger role, especially in small fields, which have a limited potential to devote land to extending or adding an SWF,

mitigating excess heat.

It is important to consider also the limitation of LST data used in the study. The Landsat LST data frequency can often be affected by clouds, which can significantly impact the availability of the data (Weng and Fu, 2014). Furthermore, this availability ranges from year to year, adding additional challenge to the assessment and transferability from one year to another. Nevertheless, creating composites (Weng and Fu, 2014; Hu et al., 2020) has been an accepted solution for building continuous data that can be further used as an input to ML models, which has been effective solution in our study as well. The incorporation of additional thermal data can further increase density of time series (Anderson et al., 2021). Another challenge for the analysis is the spatial resolution of the LST data as it can also limit the assessment of any small-scale impact of SWFs on LST. Future research could benefit from integrating high-resolution data, for instance, thermal imagery obtained from unoccupied aerial vehicles (UAVs). Despite certain limitations, our current study demonstrates the effectiveness of using Landsat-derived LST data for regional-scale analysis.

4.3. The effect of the eccentricity and orientation of small woody features

In both approaches, eccentricity of the SWF had the highest impact in the hottest year. The high values of eccentricity in this study refer to the more elliptic, which this range of value contributed positively to the model prediction. Eccentricity in the majority of the SWFs in our study ranged between 0.6 and 0.8. This means that the dataset mainly included linear SWF, and a few circular patchy woody features. Also this feature reflects the impact it has on the penetration of sunlight direction, and the wind speed and direction, which was ranked as a highly important feature in both the MLR and ML models. The analysis of Shapley values has revealed a negative impact of eccentricity on LST, suggesting that linear-shaped SWFs with higher eccentricity values have a more favourable influence. This finding implies that linear SWFs configuration to the field tend to have a more beneficial effect on LST compared to patchy ones. Hence, field management practices should consider this shape aspect to optimize their influence on LST and other related factors.

Orientation of the SWF – had no impact on MLR. In contrast, it was ranked as an important feature of ML methods and according to the Shapley value analysis (refer to Fig. 7), it indicates a positive impact of the SWF on LST. Considering both the average orientation of the SWF and the Shapley value, the effective orientation of the SWF in this region lies within the northwest to southeast range, specifically between 100 and 180°. The study by Donat et al., 2023 in a field-scale study in Brandenburg approves that the north-south orientation of tree rows in integrated in cropping systems (agroforestry) significantly impacts efficient field management, including cultivation direction, wind and water erosion, and shading.

In MLR, the size of SWF did not show any significant influence, but in both ML models, it ranked second in importance, which is not surprising, as larger SWFs can have a stronger effect. On the other hand, when examining the direction of SWF refer to the side where LST was selected and the crop types, ML methods displayed low influence, while MLR exhibited high influence. Notably, the impact of both attributes increased in 2018 and 2019, which were two years with higher average LST during the warm period. Considering this study is not a control field experience, all outcomes can be attributed to the prevailing topographical and ecological conditions in the region.

Soudouhi et al. (2018) in their study demonstrated how the consideration of the shape and orientation of green spaces produced a strong cooling effect and improved the microclimate. They found the optimal orientation occurs by considering it to be parallel to the prevailing wind. Unfortunately, a high-resolution map of wind speed and direction was not available at the regional scale to provide useful information for better field management decisions. The study by Sanusi et al. (2016) also confirmed the role of street orientation on microclimatic benefits by

influencing the duration and timing of solar radiation interception according to the sun's zenith. They suggested that the higher percentage of tree canopy could improve thermal comfort rather than the lower percentage of canopy cover (Pearlmutter et al., 2007). This information was defined in Copernicus (2019) as the compactness criterion, which in this study was mainly less or equal to 0.75. However, the outcomes of our study support the assumption that the implementation of SWF in the agricultural landscape or agroforestry is a promising approach to increasing the resilience of agricultural land against the growing occurrence of heat waves.

While we acknowledge the shortcomings of our study (a lack of information on agricultural management and soil properties, data from only one point in time during the day, and neglect of the effect of the sun's zenith), still these results have the potential to be used for decision-making on the rearrangement of SWFs within a landscape to optimize the field climate. Furthermore, the method we employed utilizes publicly available data, making it applicable in various regions with different topography. This broadens the potential for practical application and impact in diverse geographical settings.

5. Conclusion

In this study, we successfully quantified the impact of SWFs on LST in an agricultural area at the mesoscale. This method is applicable wherever the necessary data are available and accessible and provide insights for decision-makers in regional scale. We showed that a possible cooling effect of an SWF on adjacent fields manifests mainly in the short distance between 1 m and 50 m, and usually fades out beyond 75 m. The physical attributes of SWFs, such as eccentricity and orientation, can amplify this effect. In the case of eccentricity, a more elliptical shape has a greater impact. We assume that access to additional information on agricultural management (e.g. irrigation practices and crop rotation) would further improve the model performance. Confirmation of this hypothesis is still pending.

The analysis of SWFs at different distances suggests that if the LST of a relatively flat landscape in central Europe is to be regulated by planting additional trees, a significant cooling effect can be expected if trees are planted at distances less than 75 m. This supports the assumption that the implementation of agroforestry is a promising approach to increasing the resilience of agricultural land against the growing occurrence of heat waves. Aligned with the European Union's new common agricultural policy (CAP) and its focus on 'eco-schemes', decision-makers at both field and regional levels can utilize this information to improve the efficiency of agroforestry implementation. The methodology presented in this study offers the advantage of being reproducible and addresses a scale that is seldom investigated, thereby providing valuable insight for decision-makers to protect their crops against damages from extreme temperatures during summer.

CRedit authorship contribution statement

Fatemeh Ghafarian: Conceptualization, Formal analysis, Methodology, Validation, Visualization, Writing – original draft, Writing – review & editing. **Gohar Ghazaryan:** Conceptualization, Data curation, Formal analysis, Supervision, Writing – review & editing. **Ralf Wieland:** Data curation, Methodology, Supervision, Validation, Visualization. **Claas Nendel:** Conceptualization, Funding acquisition, Supervision, Writing – review & editing.

Declaration of competing interest

The authors declare that they have no known competing financial interests or personal relationships that could have appeared to influence the work reported in this paper.

Data availability

Data will be made available on request.

Acknowledgments

The investigations were conducted within the “Agricultural System of the Future: DAKIS – Digital Agricultural Knowledge and Information System” project, which was funded by the Federal Ministry of Education and Research, Germany (BMBF Förderprogramm Agrarsysteme der Zukunft – 031B0729A).

Supplementary materials

Supplementary material associated with this article can be found, in the online version, at doi:10.1016/j.agrformet.2024.109949.

References

- de Abreu-Harbach, L.V., Labaki, L.C., Matzarakis, A., 2015. Effect of tree planting design and tree species on human thermal comfort in the tropics. *Landscape Urban. Plan.* 138, 99–109. <https://doi.org/10.1016/j.landurbplan.2015.02.008>. Elsevier B.V.
- Amt für Statistik Berlin-Brandenburg (2016) Struktur der land- und forstwirtschaftlichen Betriebe, EVAS: 41121. Potsdam. Available at: <https://www.statistik-berlin-brandenburg.de/>.
- Anderson, M.C., et al., 2021. Interoperability of ECOSTRESS and Landsat for mapping evapotranspiration time series at sub-field scales. *Remote Sens. Environ.* 252, 112189. Elsevier.
- Asseng, S., et al., 2015. Rising temperatures reduce global wheat production. *Nat. Clim. Chang.* 5 (2), 143–147. Nature Publishing Group.
- Baker, T.P., et al., 2021. Temporal, environmental and spatial changes in the effect of windbreaks on pasture microclimate. *Agric. For. Meteorol.* 297, 108265. Elsevier.
- Bassa, M., et al., 2012. Factors affecting plant species richness in field boundaries in the Mediterranean region. *Biodivers. Conserv.* 21 (4), 1101–1114. <https://doi.org/10.1007/S10531-012-0245-Y/FIGURES/4>. Springer.
- Beilouin, D., et al., 2020. Impact of extreme weather conditions on European crop production in 2018: random forest - Yield anomalies. *Philos. Trans. R. Soc. B: Biol. Sci.* 375 (1810) <https://doi.org/10.1098/rstb.2019.0510>.
- Blickensdörfer, L., et al., 2022. Mapping of crop types and crop sequences with combined time series of Sentinel-1, Sentinel-2 and Landsat 8 data for Germany. *Remote Sens. Environ.* 269 (January), 112831 <https://doi.org/10.1016/j.rse.2021.112831>. Elsevier Inc.
- Bonan, G., 2016. *Ecological Climatology: Concepts and Applications*, 3rd. Cambridge University Press. Available at: https://books.google.de/books?hl=de&lr=&id=kq8kDQAAQBAJ&oi=fnd&pg=PR17&ots=s1To3FbDQO&sig=0YHv7C3qp-ziT4KTDMT9rvmwDS4&redir_esc=y#v=onepage&q&f=false. Accessed: 4 September 2022.
- Bramer, I., et al., 2018. Advances in monitoring and modelling climate at ecologically relevant scales. *Advances in Ecological Research*. Elsevier, pp. 101–161.
- Brandle, J.R., Hodges, L., Zhou, X.H., 2004. *Windbreaks in North American Agricultural Systems*. Springer Netherlands.
- Breiman, L. (2013) "Random Forests _ Enhanced Reader.pdf". Available at: <https://link.springer.com/article/10.1023/A:1010933404324>.
- Brenner, A.J., Jarvis, P.G., van den Beldt, R.J., 1995. Windbreak-crop interactions in the Sahel. 1. Dependence of shelter on field conditions. *Agric. For. Meteorol.* 75 (4), 215–234. [https://doi.org/10.1016/0168-1923\(94\)02217-8](https://doi.org/10.1016/0168-1923(94)02217-8).
- Cleugh, H.A., 1998a. Effects of windbreaks on airflow, microclimates and crop yields. *Agric. For. Meteorol.* 91 (1), 55–84. <https://doi.org/10.1023/A:1006019805109>, 1998 41: 1Springer.
- Copernicus (2019) Copernicus Land Monitoring Service High Resolution land cover characteristics. Small Woody Features 2015 reference year, Copernicus team at EEA. Available at: <https://doi.org/10.2909/4e92b07d-48b0-4a53-9db2-fd8d07070cc1>.
- Davis, K.T., et al., 2019. Wildfires and climate change push low-elevation forests across a critical climate threshold for tree regeneration. In: Proceedings of the National Academy of Sciences of the United States of America. National Academy of Sciences, 116, pp. 6193–6198. https://doi.org/10.1073/PNAS.1815107116/SUPPL_FILE/PNAS.1815107116.SAPP.PDF.
- De Frenne, P., et al., 2019. Global buffering of temperatures under forest canopies. *Nat. Ecol. Evol.* 10 <https://doi.org/10.1038/s41559-019-0842-1>.
- Donjadede, S., et al., 2010. Effects of vertical hedge interval of vetiver grass on erosion on steep agricultural lands. *Land Degrad. Dev.* 21 (3), 219–227. <https://doi.org/10.1002/LDR.900>.
- Dumortier, J., Carriquiry, M., Elobeid, A., 2021. Impact of climate change on global agricultural markets under different shared socioeconomic pathways. *Agric. Econ.* 52 (6), 963–984. Wiley Online Library.
- Donat, M., et al., 2023. Orientation of tree rows in alley cropping systems matters - The •ShadOTZ modelling tool for tree growth and shading effects. *MethodsX.* 11, 102282 <https://doi.org/10.1016/j.mex.2023.102282>.

- Ermida, S.L., et al., 2020. Google earth engine open-source code for land surface temperature estimation from the landsat series. *Rem. Sens. (Basel)* 12 (9), 1–21. <https://doi.org/10.3390/RS12091471>.
- Fisher, R.A., 1925. Theory of statistical estimation. In: *Mathematical proceedings of the Cambridge philosophical society*. Cambridge University Press, pp. 700–725.
- Franz, H., Born, K.M. and Plieninger, T. (2010) 'Landscape change and regional identity: introduction to the special section', <https://doi.org/10.1080/01426397.2010.486858>. Routledge, 35(4), pp. 427–430. <http://doi.org/10.1080/01426397.2010.486858>.
- Fraucqueur, L., et al., 2019. A new copernicus high resolution layer at pan-European scale: small woody features. *Rem. Sens. Agric., Ecosyst. Hydrol.* XXI 11149 (October), 111490X. <https://doi.org/10.1117/12.2532853>.
- Gao, Z., Gao, W., Chang, N.-B., 2011. Integrating temperature vegetation dryness index (TVDI) and regional water stress index (RWSI) for drought assessment with the aid of LANDSAT TM/ETM+ images. *Int. J. Appl. Earth Observ. Geoinf.* 13 (3), 495–503. Elsevier.
- Gaully, M., Ammer, S., 2020. Challenges for dairy cow production systems arising from climate changes. *Animal*. 14 (S1), s196–s203. Cambridge University Press.
- Geurts, P., Ernst, D., Wehenkel, L., 2006. Extremely randomized trees. *Mach. Learn.* 63, 3–42. <https://doi.org/10.1007/s10994-006-6226-1>. Springer Available at:
- Gomez-del-Campo, M., 2010. Physiological and growth responses to irrigation of a newly established hedgerow olive orchard. *HortScience. Am. Soc. Hortic. Sci.* 45 (5), 809–814. <https://doi.org/10.21273/HORTSCI.45.5.809>.
- Good, E.J., et al., 2017. A spatiotemporal analysis of the relationship between near-surface air temperature and satellite land surface temperatures using 17 years of data from the ATSR series. *J. Geophys. Res.: Atmos.* 122 (17), 9185–9210. <https://doi.org/10.1002/2017JD026880>.
- Hatfield, J.L., et al., 2020. Indicators of climate change in agricultural systems. *Clim. Change* 163, 1719–1732. Springer.
- Heisler, G.M., Dewalle, D.R., 1988. '2. Effects of windbreak structure on wind flow. *Agric. Ecosyst. Environ.* 22–23 (C), 41–69. [https://doi.org/10.1016/0167-8809\(88\)90007-2](https://doi.org/10.1016/0167-8809(88)90007-2). Elsevier.
- Hu, L., et al., 2020. Improved estimates of monthly land surface temperature from MODIS using a diurnal temperature cycle (DTC) model. *ISPRS J. Photogramm. Rem. Sens.* 168, 131–140. Elsevier.
- John, V., et al., 2016. Real-time lane estimation using deep features and extra trees regression. In: *Image and Video Technology: 7th Pacific-Rim Symposium, PSIVT 2015*. Auckland, New Zealand. Springer, pp. 721–733. November 25–27, 2015, Revised Selected Papers 7.
- Kanzler, M., et al., 2019. Microclimate effects on evaporation and winter wheat (*Triticum aestivum* L.) yield within a temperate agroforestry system. *Agrofor. Syst.* 93 (5), 1821–1841. <https://doi.org/10.1007/S10457-018-0289-4/FIGURES/8>. Springer Netherlands.
- Kaiser, T., et al., 2010. Validation of grassland indicator species selected for result-oriented agri-environmental schemes. *Biodivers. Conserv.* 19 (5), 1297–1314. <https://doi.org/10.1007/s10531-009-9762-8>.
- Karnieli, A., et al., 2010. Use of NDVI and land surface temperature for drought assessment: merits and limitations. *J. Clim.* 23 (3), 618–633.
- Keenan, T.F., Riley, W.J., 2018. Greening of the land surface in the world's cold regions consistent with recent warming. *Nat. Clim. Chang.* 8 (9), 825–828. Nature Publishing Group UK London.
- Khanal, S., Fulton, J., Shearer, S., 2017. An overview of current and potential applications of thermal remote sensing in precision agriculture. *Comput. Electron. Agric.* 139, 22–32. Elsevier.
- Kho, R.M., et al., 2001. Separating the effects of trees on crops: the case of *Faidherbia albida* and millet in Niger. *Agrofor. Syst.* 52 (3), 219–238. <https://doi.org/10.1023/A:1011820412140>.
- Kottek, M., et al., 2006. World map of the Köppen-Geiger climate classification updated. *Meteorol. Zeitsch.* 15 (3), 259–263. <https://doi.org/10.1127/0941-2948/2006/0130>.
- Kuhn, M., Johnson, K., 2013. *Applied Predictive Modeling*. Springer.
- Lüttger, A.B., Feike, T., 2018. Development of heat and drought related extreme weather events and their effect on winter wheat yields in Germany. *Theor. Appl. Climatol.* 132 (1–2), 15–29. <https://doi.org/10.1007/s00704-017-2076-y>. Theoretical and Applied Climatology.
- McNaughton, K.G., 1988. 1. Effects of windbreaks on turbulent transport and microclimate. *Agric. Ecosyst. Environ.* 22–23 (C), 17–39. [https://doi.org/10.1016/0167-8809\(88\)90006-0](https://doi.org/10.1016/0167-8809(88)90006-0). Elsevier.
- Monteith, J.L., Ong, C.K., Corlett, J.E., 1991. Soil-plant interactions in agroforestry systems. *For. Ecol. Manage.* 45 (1–4), 127–152. [https://doi.org/10.1016/0378-1127\(91\)90212-E](https://doi.org/10.1016/0378-1127(91)90212-E).
- Montgomery, I., Caruso, T., Reid, N., 2020. Hedgerows as ecosystems: service delivery, management, and restoration. *Annu Rev. Ecol. Evol. Syst.* 51, 81–102. <https://doi.org/10.1146/annurev-ecolsys-012120-100346>.
- Mutiibwa, D., Strachan, S., Albright, T., 2015. Land surface temperature and surface air temperature in complex terrain. *IEEe J. Sel. Top. Appl. Earth. Obs. Remote Sens.* 8 (10), 4762–4774. IEEE.
- Pearlmutter, D., Berliner, P., Shaviv, E., 2007. Integrated modeling of pedestrian energy exchange and thermal comfort in urban street canyons. *Build. Environ.* 42 (6), 2396–2409. Elsevier.
- Plieninger, T., 2011. Capitalizing on the carbon sequestration potential of agroforestry in Germany's agricultural landscapes: realigning the climate change mitigation and landscape conservation agendas. *Landsc. Res.* 36 (4), 435–454. <https://doi.org/10.1080/01426397.2011.582943>.
- Pouyan, S., et al., 2022. Spatial and seasonal modeling of the land surface temperature using random forest. *Computers in Earth and Environmental Sciences*. Elsevier, pp. 221–234.
- Rezaei, E.E., et al., 2023. Climate change impacts on crop yields. *Nat. Rev. Earth Environ.* 1–16. Nature Publishing Group UK London.
- Ridgeaway, G., 2007. Generalized Boosted Models: a guide to the gbm package. Update 1 (1), 2007.
- Swieter, A., Langhof, M., Lamerre, J., 2022. Competition, stress and benefits: trees and crops in the transition zone of a temperate short rotation alley cropping agroforestry system. *J. Agron. Crop. Sci.* 208 (2), 209–224. <https://doi.org/10.1111/jac.12553>.
- Sanusi, R., et al., 2016. Street orientation and side of the street greatly influence the microclimatic benefits street trees can provide in summer. *J. Environ. Qual.* 45 (1), 167–174. <https://doi.org/10.2134/jeq2015.01.0039>.
- Sayago, S., Ovando, G., Bocco, M., 2017. Landsat images and crop model for evaluating water stress of rainfed soybean. *Remote Sens. Environ.* 198, 30–39. <https://doi.org/10.1016/j.rse.2017.05.008>. Elsevier Inc.
- Senay, G.B., et al., 2019. Long-term (1986–2015) crop water use characterization over the upper Rio Grande Basin of United States and Mexico using Landsat-based evapotranspiration. *Remote Sens. (Basel)*. <https://doi.org/10.3390/rs11131587>.
- Shapiro, S.S., Wilk, M., 1965. An analysis of variance test for normality (complete samples). *Biometrika* 52 (3/4), 591. <https://doi.org/10.2307/2333709>. JSTOR.
- Skipper, S., Perktold, J., 2010. Stats models: econometric and statistical modeling with python. In: *Proceedings of the 9th Python in Science Conference*. Available at: <https://www.statsmodels.org/stable/index.html#citation>. Accessed: 13 June 2022.
- Sodoudi, S., et al., 2018. The influence of spatial configuration of green areas on microclimate and thermal comfort. *Urban For. Urban Green.* 34 (June), 85–96. <https://doi.org/10.1016/j.ufug.2018.06.002>.
- Tamang, B., Andreu, M.G., Rockwood, D.L., 2010. Microclimate patterns on the leeward side of single-row tree windbreaks during different weather conditions in Florida farms: implications for improved crop production. *Agrofor. Syst.* 79, 111–122. Springer.
- Vanneste, T., et al., 2020. Contrasting microclimates among hedgerows and woodlands across temperate Europe. *Agric. For. Meteorol.* 281 (October 2019), 107818 <https://doi.org/10.1016/j.agrformet.2019.107818>. Elsevier.
- Villan, A.F., 2019. Mastering OpenCV 4 with Python: A practical Guide Covering Topics from Image ... - Alberto Fernández Villán - Google Books. Packt Publishing Ltd. Available at: https://books.google.de/books?hl=en&lr=&id=w86PDwAAQBAJ&oi=fnd&pg=PP1&dq=Mastering+OpenCV4+with+Python,+Alberto+Fernandez+villan&ots=q2FbGp-btc&sig=mK8Ai_ko_UQPz2niLolveoEUEVQ#v=onepage&q=MasteringOpenCV4withPython%2CAlbertoFernandezvillan&f=false. Accessed: 21 July 2022.
- Virnodkar, S.S., et al., 2020. Remote Sensing and Machine Learning for Crop Water Stress Determination in Various Crops: a Critical Review, *Precision Agriculture*. Springer US. <https://doi.org/10.1007/s11119-020-09711-9>.
- Webber, H., et al., 2020. No perfect storm for crop yield failure in Germany. *Environ. Res. Lett.* 15 (10) <https://doi.org/10.1088/1748-9326/aba2a4>.
- Weiss, M., Jacob, F., Duveiller, G., 2020. Remote sensing for agricultural applications: a meta-review. *Rem. Sens. Environ.* 236 (December 2018), 111402 <https://doi.org/10.1016/j.rse.2019.111402>. Elsevier.
- Weng, Q., Fu, P., 2014. Modeling annual parameters of clear-sky land surface temperature variations and evaluating the impact of cloud cover using time series of Landsat TIR data. *Rem. Sens. Environ.* 140, 267–278. Elsevier.
- Zhang, Y., Middel, A., Turner, B.L., 2019. Evaluating the effect of 3D urban form on neighborhood land surface temperature using Google Street View and geographically weighted regression. *Landsc. Ecol.* 34 (3), 681–697. <https://doi.org/10.1007/s10980-019-00794-y>. Springer Netherlands.
- Zhu, P., Burney, J., 2022. Untangling irrigation effects on maize water and heat stress alleviation using satellite data. *Hydrol. Earth. Syst. Sci.* 26 (3), 827–840. <https://doi.org/10.5194/hess-26-827-2022>.